Hygromechanical Deformation of Wood Cell Walls Regulated by the Microfibril Angle

RongZhuang Song,[1†] ZeZhou He,[1†] JiaHao Li,[1] YuanZhen Hou,[1] HengAn Wu,[1] YinBo Zhu[1]*

[1]CAS Key Laboratory of Mechanical Behavior and Design of Materials, Department of Modern Mechanics, University of Science and Technology of China, Hefei 230027, China

[†]These authors contributed equally to this work.
*Corresponding Author. Email address: zhuyinbo@ustc.edu.cn

S1. Infinite extension modeling of the S2 layer

1. Rationale of Molecular Simulations

In this study, periodic boundary conditions (PBC) were applied in LAMMPS, along with covalent bonds across boundaries, to simulate the swelling behavior of cell wall structures, specifically in the S2 layer. While the system is not truly "infinite," it effectively mimics infinite extension by repeating a finite structural unit along a given direction.

Physical interpretation of periodic boundary conditions

In PBC, the simulation box represents a repeating unit of the material. This unit is infinitely replicated in space, but its physical properties—such as size and atomic positions—can change over time in response to external conditions. As the system swells, the finite unit within the simulation box deforms due to external factors, such as water absorption, generating strain even though the system is modeled as "infinitely long" in one direction.

Box size as an indicator of microscopic changes

PBC ensures structural continuity at the boundaries, but the local stress and strain are still observed in the deformation of individual units. Even though the "infinite length" is achieved through repeated finite units, changes in the size of a single simulation box provide insight into macroscopic structural behavior. For example, while swelling occurs at the microscopic level within the cell wall, this localized expansion also leads to the overall expansion of the simulation box, thereby generating strain.

Localized Strain Behavior

Although the structure is modeled as infinitely extended, strain remains a localized phenomenon, reflected in the size changes of the finite unit during swelling. The expansion of the cell wall material at the microscopic level translates into a measurable increase in box size, which can be used to quantify strain.

In conclusion, Periodic boundary conditions allow for the simulation of infinite extension by replicating a finite unit, providing a way to study the swelling behavior of

the wood cell wall. Even though the system is modeled as infinitely long, localized swelling leads to measurable strain in the finite units, making it reasonable to calculate strain based on box size changes under PBC.

2. Formation of Periodic Boundaries

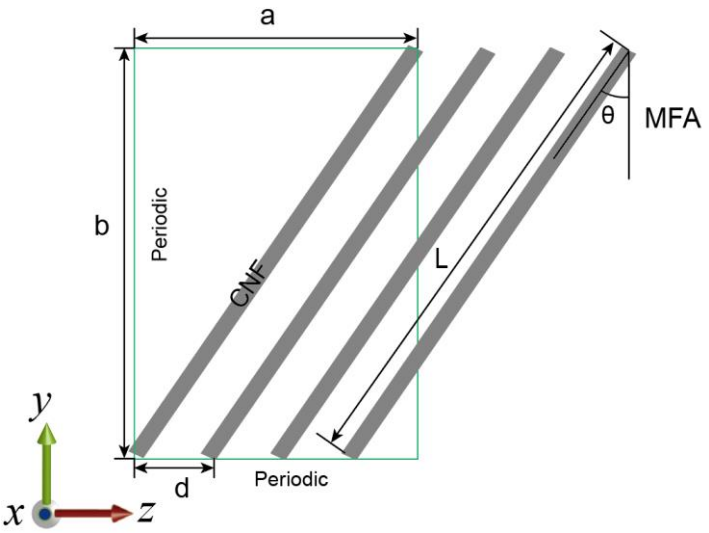

Figure S1. Schematic diagram of structural periodicity

In this simulation, periodic boundary conditions (PBC) are applied in the x, y, and z directions (Figure S1), with hemicellulose distributed between CNFs. The CHARMM potential field is employed to model molecular interactions, ensuring that the c-axis of the CNFs remains periodic, thereby preserving covalent bonds across boundaries. The simulation box size is carefully controlled to prevent the overlap of CNFs along the axial direction while allowing bond angles to properly connect the structures. Under the CHARMM force field, the rotation of CNF and changes in the simulation box size can lead to variations in the bond lengths of the CNFs. Therefore, for each given MFA, the length L of a single CNF, the number of fibers N within the box, and the spacing d between the CNFs must all be determined. A necessary condition for this is that

$$d < a/N \qquad (1)$$

where a represents the length of the simulation box in the z-direction. To achieve real periodicity and maintain proper bonding at the boundaries, extensive parameter adjustments are required for each MFA, ensuring the bonds at the boundaries remain intact throughout the simulation between CNFs at various MFAs. Table S2 presents the

length (L), the number of CNFs (N), the thickness of CNFs (H), the spacing (d), and the box sizes (a and b) at various MFAs. Figures S2-S5 illustrate the structure of each unit cell at different MFAs, along with the covalent bonding at the periodic boundaries after replication along the y and z directions. As the MFA changes, both the box size and the spacing between units vary accordingly. The covalent bonds at the boundaries are correctly connected, confirming that the periodicity of all structures is accurate and properly maintained.

Table S1. Parameter settings of the unit cell at different MFAs

θ (°)	L (Å)	H (Å)	N	d (Å)	a (Å)	b (Å)	Mass ratio of CNF to hemicellulose
0	155.7	36.8	2	40	75.8	156.4	4:1
7.5	519	36.8	2	36	73.5	515.6	4:1
15	570.9	36.8	2	37	74	551	4:1
22.5	394.4	36.8	2	38.5	77	363.2	4:1
30	342.5	36.8	2	42.7	85.6	296.7	4:1
37.5	145.3	36.8	2	44.8	89.5	114.5	4:1
45	134.9	36.8	2	47.7	95.4	95.4	4:1

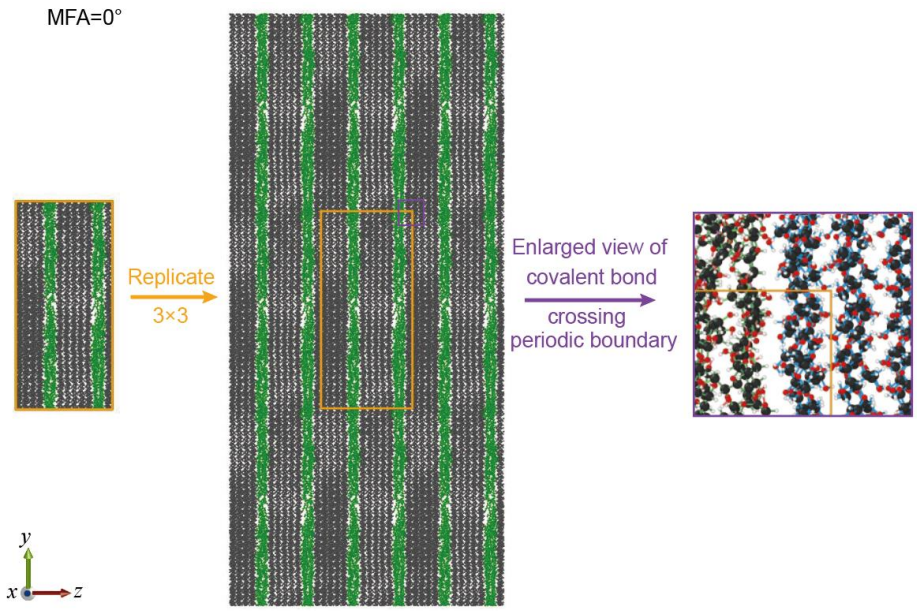

Figure S2. Schematic diagram illustrating the model's periodic boundary conditions. The initial unit cell, with a microfibril angle (MFA) of 0° (left), is expanded threefold in both the y and z directions (right). Covalent bonds at the boundaries are

highlighted and magnified in the purple box. Covalent bonds within the CNFs and hemicellulose are marked in blue and green, respectively.

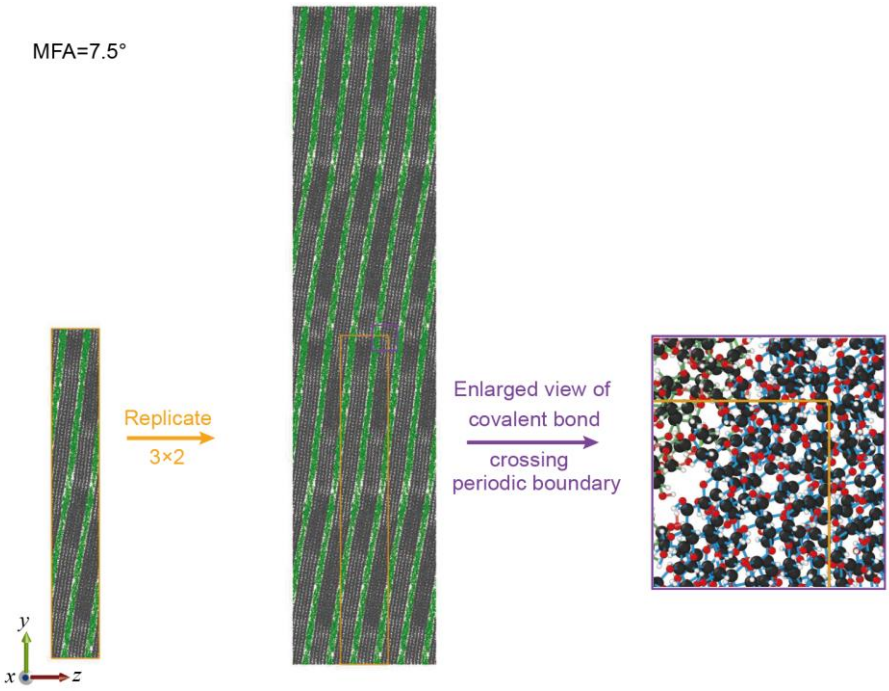

Figure S3. Schematic diagram illustrating the model's periodic boundary conditions. The initial unit cell, with a microfibril angle (MFA) of 7.5° (left), is expanded threefold in the z direction and twofold in the y direction (right). Covalent bonds at the boundaries are highlighted and magnified in the purple box. Covalent bonds within the CNFs and hemicellulose are marked in blue and green, respectively.

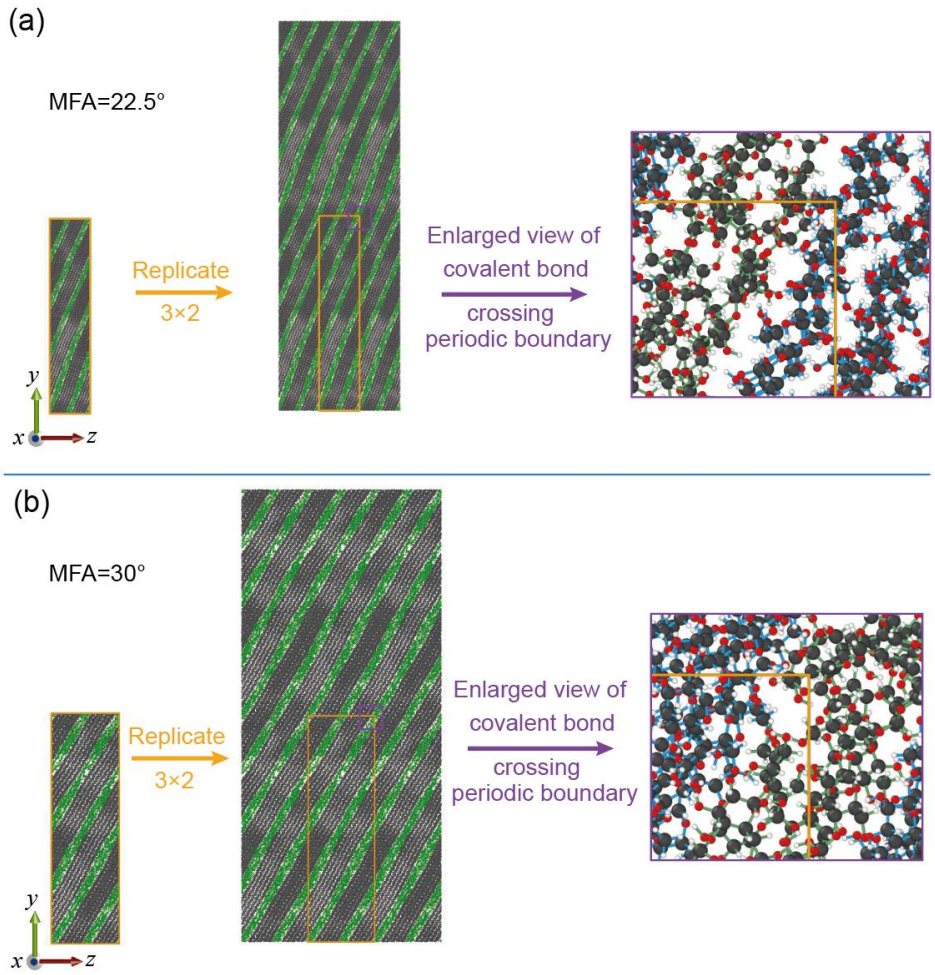

Figure S4. Schematic diagram illustrating the model's periodic boundary conditions. The initial unit cells, with microfibril angle (MFA) of 22.5° (a) and 30° (b), are expanded threefold in the z direction and twofold in the y direction. Covalent bonds at the boundaries are highlighted and magnified in the purple box. Covalent bonds within the CNFs and hemicellulose are marked in blue and green, respectively.

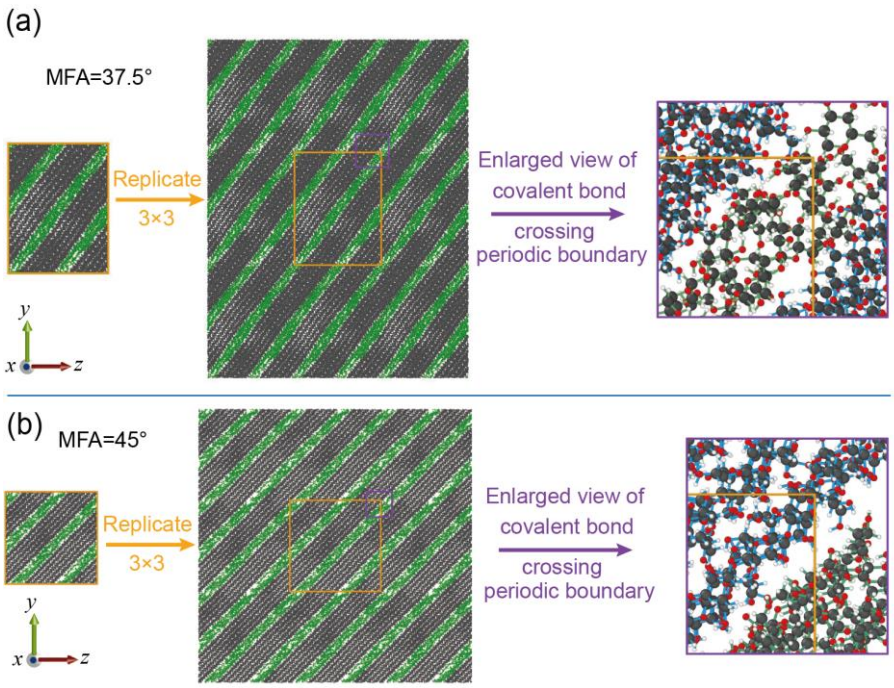

Figure S5. Schematic diagram illustrating the model's periodic boundary conditions. The initial unit cells, with microfibril angle (MFA) of 37.5° (a) and 45° (b), are expanded threefold in both the y and z directions. Covalent bonds at the boundaries are highlighted and magnified in the purple box. Covalent bonds within the CNFs and hemicellulose are marked in blue and green, respectively.

S2. Hydration-induced deformation

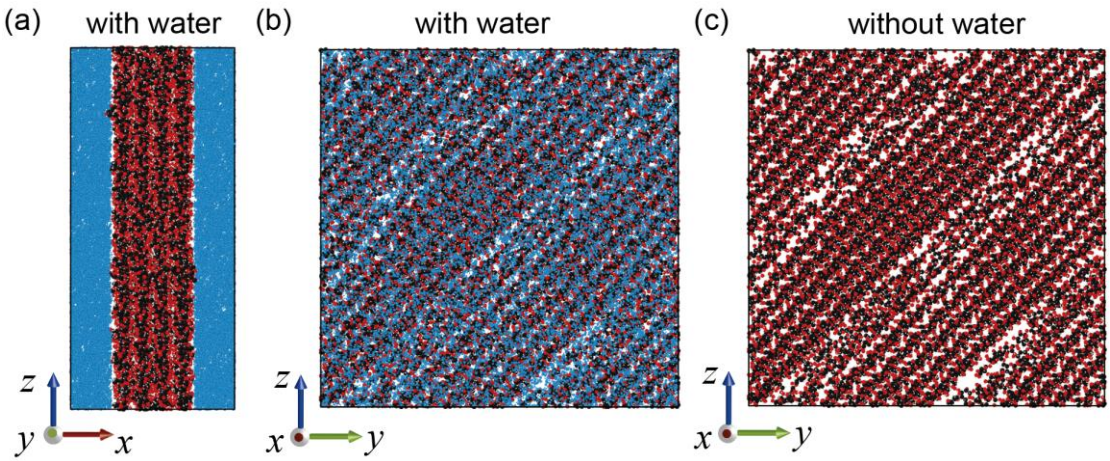

Figure S6. Schematic of the model at the initial stage of infiltration. MFA = 45° is taken as an example. (a,b) Configurations on different planes with water molecules. (c) Configuration on y-z plane without water molecules.

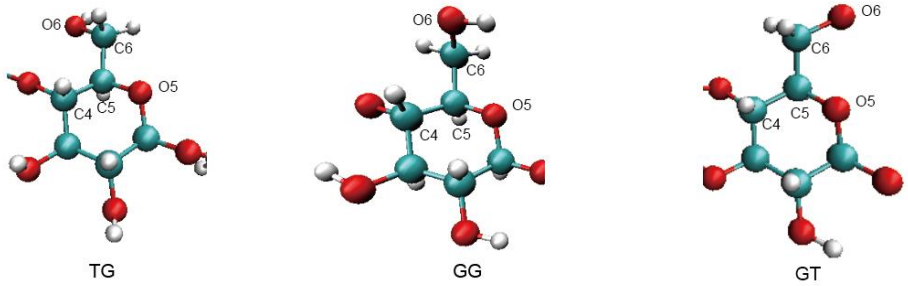

Figure S7. Schematic diagram of the three conformations of TG, GG, and GT.

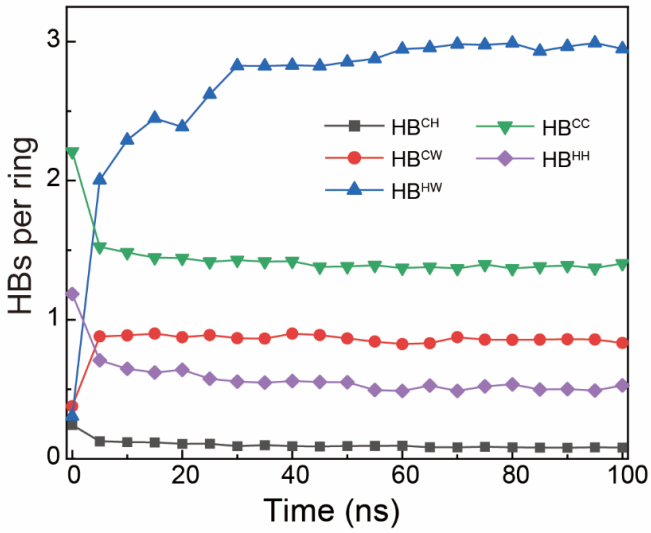

Figure S8. The number of different types of HBs per ring varies with wetting time

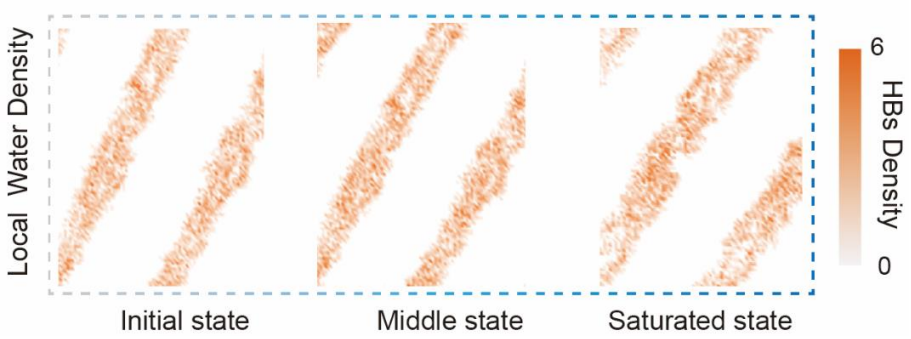

Figure S9. Regional density distribution of hemicellulose with water addition time.

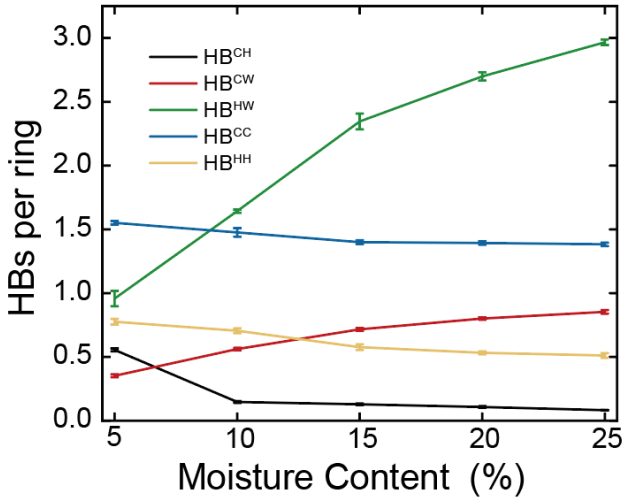

Figure S10. The number of different types of HBs per ring varies with moisture, Here MFA = 22.5° is selected as an example.

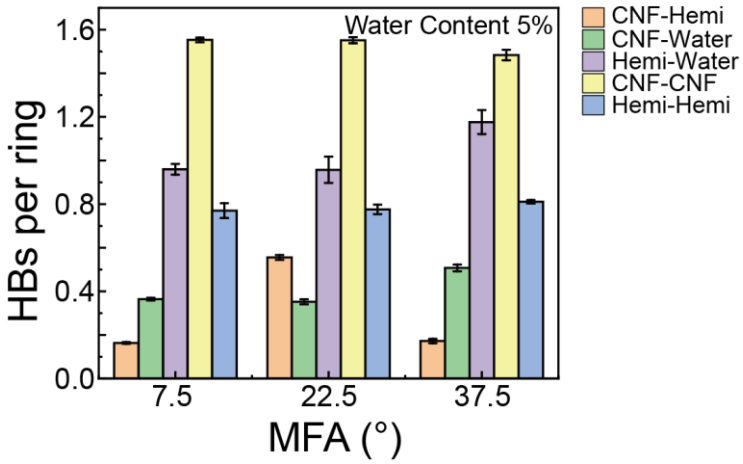

Figure S11. The number of each type of HBs per ring as a function of microfibril angles with a moisture content of 5%. Error bars correspond to standard deviation.

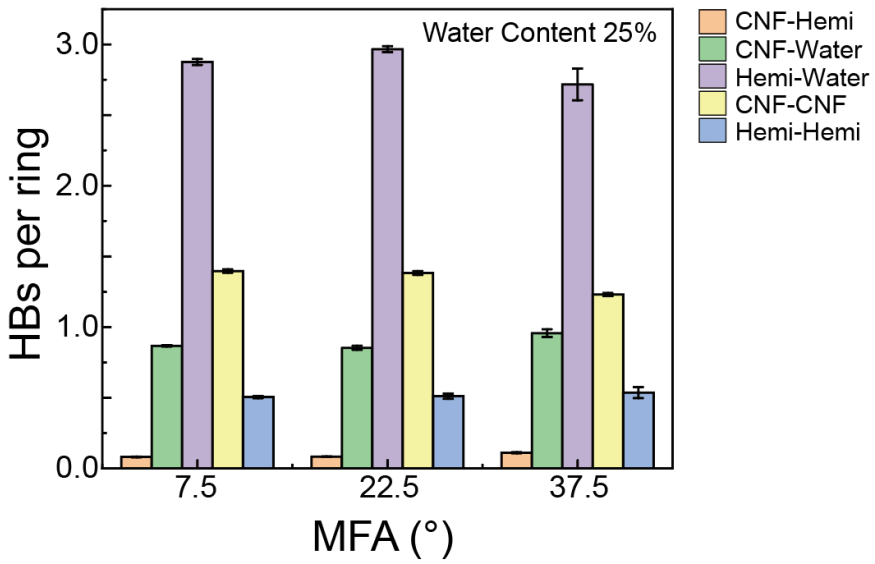

Figure S12. The number of each type of HBs per ring as a function of microfibril angles with a moisture content of 25%. Error bars correspond to standard deviation.

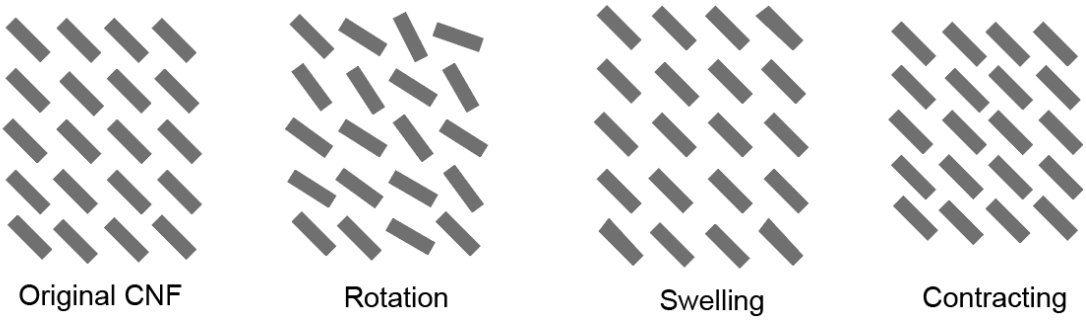

Figure S13. Schematic diagram of different deformation types of CNF.

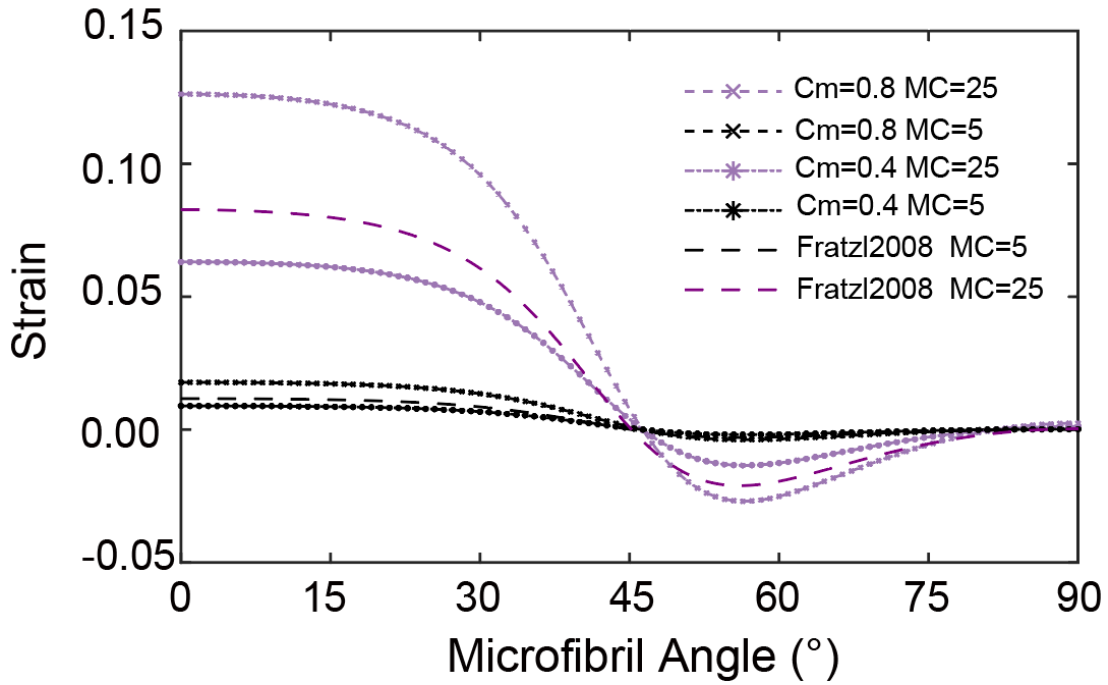

Figure S14. Comparison of strain prediction curves between the Fratzl model and mixed rule analysis.

Table S2. Experimental Data on Hygromechanical Deformation in Wood Cell Walls Regulated by Microfibril Angle

Reference	Wood Type	Microfibril Angle (MFA)	Observed Deformation Behavior
Eur. J. Wood Prod (2010) [1]	36-year-old Sitka spruce	20° ± 5°	Maximum deformation range
Nature (2023)[2]	14-20-year-old white oak	23° ± 7°	Maximum deformation range
Nature (1997)[3]	Pine cones	16° ± 5°	Capable of elongation
Nature (1997)[3]	Pine cones	60° ± 2°	Resist elongation

S3. Mixture rule analysis

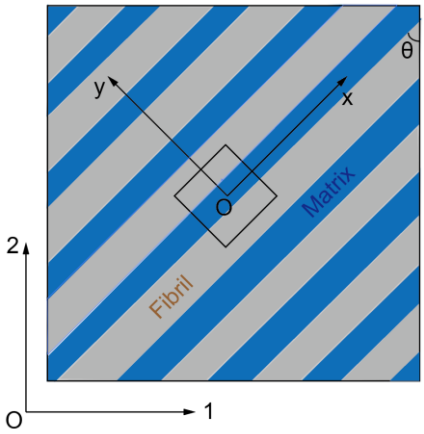

Figure S15. Two-Phase Structural Model and Coordinate System Diagram

The constitutive of fiber in x and y directions can be expressed as:

$$\begin{cases} \sigma_{Fx} = E_F \varepsilon_{Fx} \\ \sigma_{Fy} = E_F \varepsilon_{Fy} \end{cases} \tag{1}$$

Assume the swelling strain of matrix along x and y directions is η, we get the constitutive of the matrix:

$$\begin{cases} \sigma_{Mx} = \frac{E_M}{1-\nu^2}(\varepsilon_{Mx} - \eta) + \frac{\nu E_M}{1-\nu^2}(\varepsilon_{My} - \eta) \\ \sigma_{My} = \frac{\nu E_M}{1-\nu^2}(\varepsilon_{Mx} - \eta) + \frac{E_M}{1-\nu^2}(\varepsilon_{My} - \eta) \end{cases} \tag{2}$$

The stress and strain relationship between matrix and fibers can be expressed as:

$$\begin{cases} \sigma_y = c_m \sigma_{My} + (1 - c_m)\sigma_{Fy}, \sigma_x = \sigma_{Fx} = \sigma_{Mx} \\ \varepsilon_x = c_m \varepsilon_{My} + (1 - c_m)\varepsilon_{Fy}, \varepsilon_y = \varepsilon_{Fx} = \varepsilon_{Mx} \end{cases} \tag{3}$$

Combining Eqs. (1), (2) and (3), we can solve the swelling stress of Two-Phase structure:

$$\begin{cases} \sigma_x = \frac{E_F(c_m(-\eta(\nu+1)+\nu\varepsilon_y)+\varepsilon_x)}{(1-\nu^2)\varphi c_m+(1-c_m)} \\ \sigma_y = \frac{E_M\left[\left(c_m{}^2(\varphi(\nu+1)-1)\left((\nu-1)\varepsilon_y\varphi+\varepsilon_y-\eta\right)\right)+c_m\left(\nu\varepsilon_x\varphi+\varepsilon_y((\varphi-1)^2-\nu^2\varphi^2)\right)-\eta\right]}{(1-\nu^2)\varphi c_m+(1-c_m)} \end{cases} \tag{4}$$

Where φ = E_F/E_M is the modulus ratio of fibers and matrix.
Then the stress and strain in global coordinates can be expressed as the rotation of stress and strain in the material coordinates:

$$\boldsymbol{\sigma}^{\boldsymbol{g}} = \boldsymbol{R}\boldsymbol{\sigma}^{m} \tag{5}$$

Where

$$\boldsymbol{\sigma}^{\boldsymbol{g}} = \begin{bmatrix} \sigma_1 \\ \sigma_2 \\ \tau_{12} \end{bmatrix} \tag{6}$$

$$\boldsymbol{\sigma^m} = \begin{bmatrix} \sigma_x \\ \sigma_y \\ \tau_{xy} \end{bmatrix} \tag{7}$$

R represents the coordinate transformation matrix, its expanded forms are as follows:

$$R = \begin{pmatrix} cos^2\theta & sin^2\theta & 2sin\theta cos\theta \\ sin^2\theta & cos^2\theta & -2sin\theta cos\theta \\ -sin\theta cos\theta & sin\theta cos\theta & cos^2\theta - sin^2\theta \end{pmatrix} \tag{8}$$

When no external stress is applied, the Two-Phase structure will be relaxed to a stress-free configuration. To solve the swelling strain of stress-free configuration, we set the stresses of configuration equal zero and finally we get:

$$\begin{cases} \sigma_1 = 0 \\ \sigma_2 = 0 \end{cases} \tag{9}$$

Then the swelling strain ε_1 can be solved:

$$\varepsilon_1 = \frac{L_1}{L_2} \tag{10}$$

Where

$$\begin{aligned} L_1 = \eta c_m \{ & 4{c_m}^2 cos^2\theta cos2\theta(\nu\varphi + \varphi - 1)^2 \\ & - c_m(\nu\varphi + \varphi - 1)[2cos2\theta(\nu\varphi + \varphi - 2) + cos4\theta(\nu\varphi + \varphi - 1) \\ & + \nu\varphi + \varphi + 1] - 2(cos2\theta(\nu\varphi + \varphi - 1) + \nu\varphi + \varphi + 1)\} \end{aligned}$$

$$\begin{aligned} L_2 = -c_m[& cos4\theta(\nu\varphi + \varphi - 1)^2 + (-\nu^2 + 2\nu + 3)\varphi^2 + 2(\nu - 3)\varphi + 3] \\ & + {c_m}^2(\nu\varphi + \varphi - 1)[cos4\theta(\nu\varphi + \varphi - 1) - (\nu - 3)\varphi - 3] - 4\varphi \end{aligned}$$

A more detailed derivation process can be found in our forthcoming publication (Li et al. Biomimetic Turing Machine: A Multiscale Theoretical Framework for Inverse Design of Target Space Curves[J]. Available at SSRN 4936519).[4]

Here ν represents the Poisson coefficient of the hemicellulose matrix, φ represents the elastic modulus ratio of CNF and hemicellulose, c_m represents the volume fraction of hemicellulose, θ represents microfibril angle, η represents the isotropic volume strain due to swelling of the matrix, ε_1 represents swelling strain in the 1-axis direction.

References

1 M. Leonardon, C. M. Altaner, L. Vihermaa and M. C. Jarvis, *Eur. J. Wood Prod*., 2009, **68**, 87-94.

2 D. Luo, A. Maheshwari, A. Danielescu, J. Li, Y. Yang, Y. Tao, L. Y. Sun, DK. Patel, G. Y. Wang, S. H. Yang, T. Zhang, L. Yao, *Nature*, 2023, **614**, 463-470.

3 C. Dawson, J. F. V. Vincent and A. M. Rocca, *Nature*, 1997, **390**, 668.

4 J. Li, X. Sun, Z. He, Y. Hou, H. Wu and Y. Zhu, *J. Mech. Phys. Solids*, Available at SSRN 4936519. https://papers.ssrn.com/sol3/papers.cfm?abstract_id=4936519